Published in final edited form as:

Circ Res. 2017 June 09; 120(12): 1874–1888. doi:10.1161/CIRCRESAHA.116.310283.

Analysis of Cardiac Myocyte Maturation Using CASAAV, A Platform for Rapid Dissection of Cardiac Myocyte Gene Function In Vivo

Yuxuan Guo[1], **Nathan J. VanDusen**[1], **Lina Zhang**[2], **Weiliang Gu**[3], **Isha Sethi**[4], **Silvia Guatimosim**[5], **Qing Ma**[1], **Blake D. Jardin**[1], **Yulan Ai**[1], **Donghui Zhang**[1], **Biyi Chen**[6], **Ang Guo**[6], **Guo-Cheng Yuan**[4], **Long-Sheng Song**[6,7], and **William T. Pu**[1,8]

[1]Cardiology, Boston Children's Hospital, Boston, MA 02115 USA

[2]Institute of Basic Medicine, Shanghai University of Traditional Chinese Medicine, Shanghai 201203, China

[3]Pharmacology, School of Pharmacy, Shanghai University of Traditional Chinese Medicine, Shanghai 201203, China

[4]Biostatistics and Computational Biology, Dana-Farber Cancer Institute, Boston, MA 02215, USA

[5]Physiology and Biophysics, Institute of Biological Sciences, Universidade Federal de Minas Gerais, Av. Antônio Carlos 6627, Belo Horizonte, MG - CEP: 31270-901, Brazil

[6]Cardiovascular Medicine, Department of Internal Medicine, François M. Abboud Cardiovascular Research Center, University of Iowa Carver College of Medicine, Iowa City, IA 52242, USA

[7]Veterans Affairs Medical Center, Iowa City, IA 52242, USA

[8]Harvard Stem Cell Institute, Cambridge, MA 02138 USA

Abstract

Rationale—Loss-of-function studies in cardiac myocytes (CMs) are currently limited by the need for appropriate conditional knockout alleles. The factors that regulate CM maturation are poorly understood. Prior studies on CM maturation have been confounded by heart dysfunction caused by whole organ gene inactivation.

Address correspondence to: Dr. William T. Pu, Department of Cardiology, Boston Children's Hospital, 300 Longwood Ave., Boston, MA 02115, Tel: 617-919-2091, wpu@pulab.org.

*Y.G., and N.J.V. contributed equally to this work.

In February 2016, the average time from submission to first decision for all original research papers submitted to *Circulation Research* was 15.4 days.

AUTHOR CONTRIBUTIONS

YG and NJV contributed equally to this manuscript. YG designed and performed experiments and collected and analyzed data. NJV developed the somatic mutagenesis AAV vector and contributed to data collection and analysis. LZ, WG, QM, BJ, and DZ contributed to creation of reagents and collection of data. NJV and SG performed Ca^{2+} imaging. IS and GCY analyzed amplicon-seq data. AG and LSS contributed to analysis of T-tubule morphology with AutoTT software. YG and NJV wrote the manuscript. WTP directed the overall project, analyzed data, and edited the manuscript.

DISCLOSURES

The authors have no conflicts to disclose.

Objective—To develop a new technical platform to rapidly characterize cell-autonomous gene function in postnatal murine CMs and apply it to identify genes that regulate T-tubules, a hallmark of mature cardiac myocytes.

Methods and Results—We developed CASAAV (CRISPR/Cas9-AAV9-based somatic mutagenesis), a platform in which AAV9 delivers tandem guide RNAs targeting a gene of interest and cardiac troponin T promoter (cTNT)-driven Cre to *Rosa*$^{Cas9GFP/Cas9GFP}$ neonatal mice. When directed against junctophilin-2 (*Jph2*), a gene previously implicated in T-tubule maturation, we achieved efficient, rapid, and CM-specific JPH2 depletion. High-dose AAV9 ablated JPH2 in 64% CMs and caused lethal heart failure, whereas low-dose AAV9 ablated JPH2 in 22% CMs and preserved normal heart function. In the context of preserved heart function, CMs lacking JPH2 developed T-tubules that were nearly morphologically normal, indicating that JPH2 does not have a major, cell-autonomous role in T-tubule maturation. However, in hearts with severe dysfunction, both AAV-transduced and non-transduced CMs exhibited T-tubule disruption, which was more severe in the transduced subset. These data indicate that cardiac dysfunction disrupts T-tubule structure, and that JPH2 protects T-tubules in this context. We then used CASAAV to screen 8 additional genes for required, cell-autonomous roles in T-tubule formation. We identified ryanodine receptor 2 (RYR2) as a novel, cell-autonomously required T-tubule maturation factor.

Conclusions—CASAAV is a powerful tool to study cell-autonomous gene functions. Genetic mosaics are invaluable to accurately define cell-autonomous gene function. JPH2 has a minor role in normal T-tubule maturation but is required to stabilize T-tubules in the failing heart. RYR2 is a novel T-tubule maturation factor.

Keywords

Cardiac myocyte maturation; T-tubule; CRISPR/Cas9; genetic mosaic; junctophilin 2; ryanodine receptor 2 gene; development; mutation

Subject Terms

Cell Biology/Structural Biology; Developmental Biology; Genetically Altered and Transgenic Models; Basic Science Research; Myocardial Biology

INTRODUCTION

During mammalian heart development, cardiac myocyte (CM) phenotype changes dramatically between fetal, neonatal, and adult stages[1]. Fetal CMs are small, proliferative, and primarily produce energy through glycolysis. In contrast, adult CMs are much larger, terminally differentiated, and primarily produce energy through oxidative phosphorylation. The transition from fetal to adult phenotypes, referred to as CM maturation, occurs most rapidly in the perinatal period in the mouse between the end of gestation and about postnatal day 20 (P20). The mechanisms that govern CM maturation are poorly understood. Presently, maturation of stem cells or non-myocytes directed to differentiate into CMs is a major hurdle impeding the use of these technologies for disease modeling or therapeutic cardiac regeneration[1]. Understanding the factors that regulate endogenous CM maturation would facilitate efforts to overcome this hurdle.

Among the most characteristic and latest developing hallmarks of adult cardiac myocytes are transverse tubules (T-tubules), which start to form at ~P10 in mouse and become fully mature at ~P20[2]. T-tubules are tubular invaginations of the plasma membrane that penetrate deep within CMs and align with the Z-lines of sarcomeres. The junctional sarcoplasmic reticulum comes in close proximity to T-tubules at specialized membrane micro-domains known as dyads, which mediate Ca^{2+}-induced Ca^{2+} release and thereby couples cardiac myocyte electrical activity to contraction. The cardiac action potential rapidly spreads along T-tubules, where depolarization activates the L-type Ca^{2+} channel. The resulting small influx of Ca^{2+} activates ryanodine receptor 2 (RYR2), the major cardiac intracellular Ca^{2+} release channel located on the junctional SR. Activated RYR2 releases a large amount of Ca^{2+}, which induces sarcomere contraction. Thus T-tubules facilitate coordinated Ca^{2+} release within large adult CMs which could not be achieved through sequential, diffusion-mediated spread of the Ca^{2+} transient[3,4].

Although the physiological functions of T-tubules have been well characterized, the molecular machinery that induces the maturation and maintenance of T-tubules is largely unknown. Junctophilin-2 (JPH2)[5,6], a structural protein that is specifically expressed in CMs, uses its N-terminal plasma membrane binding motifs and C-terminal SR transmembrane domain to tether T-tubule and SR membrane together to form dyads[7]. CM-specific knockdown of *Jph2* in mouse caused dramatic remodeling and loss of T-tubules during postnatal development[2,8]. This result was interpreted as evidence that JPH2 is a critical regulator of T-tubule maturation[2,8]. However, JPH2 depletion in this mouse model also causes severe cardiomyopathy and heart failure[2,8]. T-tubule disruption is present in hearts with cardiomyopathy and heart failure[9–10]. Thus cardiomyopathy and heart failure confound the interpretation of the *Jph2* knockdown phenotype with regard to its role in T-tubule maturation.

The confounding effect of secondary changes caused by cardiac stress response in conventional genetic analyses is a common problem for studies of CM maturation, and indeed for cardiac biology in general. Genetic knockouts that induce cardiac dysfunction and failure precipitate a host of indirect secondary effects, and dissecting direct effects of genetic manipulations from secondary effects can be problematic. In this study, we established a platform for quickly producing genetic mosaic knockouts which allow investigation of cell-autonomous effects of gene knockout within the context of normally functioning myocardium. We deployed this platform to precisely characterize CM maturation factors without the interference of heart failure. We found that JPH2 is not required for overall T-tubule formation; rather, it helps to stabilize T-tubules in the face of cardiac dysfunction. We then use this platform and a candidate-based approach to identify novel T-tubule maturation factors. This platform will be useful for dissecting cell-autonomous genetic pathways that regulate postnatal CM maturation and function.

METHODS

Please refer to the Online Supplement for Detailed Materials and Methods.

AAV

AAV-U6gRNA-cTNT-Cre plasmid (Online Fig. I) was constructed by transferring a cTNT-Cre cassette from AAV-TNT-Cre plasmid[11] to PX552 plasmid[12]. A second U6gRNA was further added to generate AAV-U6gRNA$_1$-U6gRNA$_2$-cTNT-Cre (Addgene #87682). 20 bp gRNA sequences (Online Table I) were cloned into these plasmids through a single ligation step.

AAV was produced and purified using a standard protocol with modifications[13]. AAV titer was quantified by qPCR using primers indicated in Online Table II.

Mice

All animal procedures were approved by the Boston Children's Hospital Institutional Animal Care and Use Committee. AAVs were injected into P1 *Rosa*$^{Cas9GFP/Cas9GFP}$ mice[14] by subcutaneous injection. Cardiac myocytes were dissociated by retrograde collagenase perfusion as described previously[15].

Validation and examination of Jph2 depletion in CMs

The mRNA level of *Jph2* was examined by qRTPCR using primers shown in Online Table II. The deletion of *Jph2* between two gRNAs was detected by RT-PCR. Construction of DNA libraries for amplicon sequencing was performed by modifying a published protocol[16] using primers shown in Online Table II. Paired-end, 250 bp reads were generated on an Illumina MiSeq and analyzed using CRISPResso software[17].

Validation of gene knockout was performed through immunofluorescence. Antibodies and dyes used are listed in Online Table III. Hearts were dissociated into single CMs through retrograde collagenase perfusion. Then the CMs were briefly cultured to allow attachment to laminin-coated glass coverslips. Next the CMs were fixed by 4% PFA and immunostaining was performed as described[18,19]. Confocal images were taken using Olympus FV1000 inverted laser scanning confocal microscope equipped with a 60X/1.3 silicone-oil objective.

Flow cytometry

Quantitative analysis by flow cytometry was performed using a Propel Laboratories Avalon cytometer with a 100 μm nozzle and standard GFP/RFP filter sets. Data were further analyzed using BioRad ProSort software.

Fluorescence-activated cell sorting (FACS) was performed using a BD AriaII SORP cell sorter with a 100 μm nozzle at Dana-Farber flow cytometry core facility.

Analyses of heart phenotypes

Gross heart morphology was imaged under a stereomicroscope (Zeiss SteREO Discovery V8) with an AxioCam MRc camera. Heart histology, organ weights, and expression of cardiac stress markers were assayed as described previously[13]. Echocardiography was performed on awake animals using a VisualSonics Vevo 2100 with Vevostrain software. Echocardiography was performed blinded to AAV types and doses.

T-tubule imaging and analysis

In situ T-tubule imaging and AutoTT analysis of T-tubule patterns were performed as described previously[20].

Intracellular Ca^{2+} recording

Intracellular Ca^{2+} was measured in isolated CMs that were loaded with Rhod-2 AM. Cells were electrically stimulated at 1 Hz to produce steady-state conditions. All image data were acquired in the line scanning mode along the long axis of the cell using a Olympus FV1000 inverted laser scanning confocal microscope with a 60X/1.3 silicone-oil objective.

Statistics

Unless otherwise noted, values are displayed as mean ± standard deviation. Statistical comparisons were performed using Student's *t*-test. Kaplan-Meier survival analysis was performed using JMP software (SAS).

RESULTS

CASAAV efficiently depletes JPH2 in CMs during CM maturation

Previously our lab showed that the heart could tolerate the deletion of essential genes in a small fraction of CMs while still maintaining normal heart function[11]. This mosaic analysis allowed us to study CM maturation in individual cells without the interference of secondary effects caused by heart failure. To establish a versatile technical platform that allows mosaic somatic mutagenesis of any gene specifically in CMs, we combined adeno-associated virus (AAV)-mediated mosaic transduction[11] with clustered regularly interspaced short palindromic repeats (CRISPR)/Cas9-based in vivo mutagenesis[14,21–24]. We constructed AAV vectors that contain one or two U6-promoter-driven gRNA expression cassettes and a cardiac troponin-T (cTNT) promoter that drives CM-specific expression of Cre recombinase (Fig. 1A and Online Fig. I). Using these vectors, we generated AAV9[25], a cardiotropic AAV serotype, and subcutaneously injected the replication-deficient virus into *Rosa26*$^{Cas9\text{-}GFP}$ mice that harbor a Cre-inducible Cas9-P2A-GFP allele[14]. cTNT-Cre activated the expression of Cas9 and GFP specifically in AAV-transduced CMs, and the U6 promoter drove expression of gRNA(s) in these cells (Fig. 1A). Thus GFP^+ CMs express Cas9 nuclease activity that is directed specifically to target sites by gRNA(s). The nuclease creates DNA double strand breaks at these target sites and triggers DNA damage repair by non-homologous end-joining (NHEJ), which is error-prone and frequently results in insertions or deletions that can induce frameshift mutations silencing the targeted genes (Fig. 1A)[26].

We first designed a gRNA that targets tdTomato gene and tested whether the tdTomato protein in *Rosa*$^{Cas9\text{-}GFP/tdTomato}$ mice is depleted by this CRISPR/Cas9-AAV9-based somatic mutagenesis (CASAAV) system. We injected AAV-TNT-Cre (negative control) or AAV-gRNA(tdTomato)-TNT-Cre into postnatal day1 (P1) littermate pups and isolated CMs at 1 month by retrograde collagenase perfusion. The CMs were analyzed by flow cytometry to detect GFP and tdTomato. We found that tdTomato was depleted in ~89% GFP^+ CMs that were transduced by AAV expressing tdTomato gRNA (Fig. 1B). No depletion was detected in GFP^+ CMs transduced with control AAV that lacked gRNA (Fig. 1B and Online Fig. II).

Interestingly, while theoretically Cre should trigger expression of both Tomato and Cas9-P2A-GFP, we also detected tdTomato^{+} GFP^{-} cells (Online Fig. II). Two effects likely resulted in these cells: (1) some CMs transiently harbor AAV and limited Cre exposure activates tdTomato but not Cas9-P2A-GFP, as a result of differential sensitivity of these alleles to Cre activation; and (2) GFP level was observed to be sensitive to CM stress, as occurs during CM dissociation and flow cytometry. The net effect is that a minority of GFP^{-} cells may have undergone Cas9 genome editing, a technical factor that needs to be considered when interpreting data (see discussion). Overall, this pilot experiment demonstrates that the CASAAV system mediates highly efficient gene silencing in CMs in vivo.

Next we designed two gRNAs that target the coding sequence of *Jph2* within exon 1, which encodes the first four plasma membrane binding motifs of JPH2 protein (Fig. 1C). These gRNAs had at least 3 mismatches to any non-targeted sequences in the mouse reference genome (Online Fig. IIIA). We generated AAVs that expressed each gRNA individually (Jph2-gRNA1 or Jph2-gRNA2), or both simultaneously (Jph2-gRNA1+2), and injected 1.1 × 10^{9} vg/g (viral genomes per gram body weight) AAV into P1 Rosa$^{Cas9\text{-}GFP/Cas9\text{-}GFP}$ pups. We isolated CMs from P21 hearts and performed immunofluorescence to detect JPH2 protein (Fig. 1D). We found that Jph2-gRNA1, Jph2-gRNA2, and Jph2-gRNA1+2 depleted JPH2 immunofluorescence in ~55%, ~70%, and ~80% of GFP^{+} CMs, respectively (Fig. 1E). We also analyzed JPH2 depletion in transduced CMs by using fluorescence-activated cell sorting (FACS) to purify GFP^{+} CMs, followed by Western blot (Fig. 1F–G). Jph2-gRNA1+2 efficiently depleted JPH2 in transduced CMs. The level of BIN1, another protein implicated in T-tubule maturation[27], was not affected (Fig. 1G). The major effect of Jph2-gRNA1+2 was protein depletion rather than truncation (Online Fig. IV), although we cannot exclude production of truncated protein in a low fraction of transduced cells. Overall our data show that Jph2-CASAAV efficiently depleted JPH2 in CMs, and that two gRNAs were more efficient at achieving protein depletion than each single gRNA.

To determine the mechanisms that mediate this efficient JPH2 depletion, we injected 5.5 × 10^{10} vg/g AAV at P1, which is sufficient to transduce ~75% CMs in the heart (please refer to Fig. 3 below). At P7, we extracted RNA from heart apexes and detected significantly decreased *Jph2* mRNA after AAV-Jph2gRNA treatment by quantitative RT-PCR (qRT-PCR) (Fig. 2A–B). Analysis of *Jph2* transcript structure by RT-PCR demonstrated that dual-gRNA CASAAV induced deletion of the intervening coding sequence between two gRNA targets in a subset of transcripts, which was not observed with either gRNA alone (Fig. 2A and C). To more precisely define the effect of CASAAV on *Jph2* transcripts, we amplified each gRNA targeted site from cDNA and performed next-generation sequencing (Amplicon-Seq)[28] (Fig. 2A, 2D–F, and Online Fig. IIIB–C). Analysis of these sequences using CRISPResso[17] showed that gRNA1 alone generated mutations in 72% of transcripts, and 71% of these mutated reads shift the translational reading frame (Fig. 2D). gRNA2 alone generated mutations in 61% of transcripts, and 86% of these mutated reads shift the translational reading frame (Fig. 2D). These mutations localized to the expected gRNA cleavage sites (Fig. 2E). When both gRNAs were present, frame-shift mutations were detected in >80% mutated reads, and these mutations occurred between the two gRNA-targeted sites (Fig. 2D–F). Thus JPH2 protein depletion induced by CASAAV is due to a combination of frame-

shifting mutations and mRNA decrease, potentially resulting from nonsense-mediated decay[29]. The use of two gRNAs increased the efficiency of both of these effects. Deletion of *Jph2* coding sequences that encode critical plasma membrane binding domains between the two gRNA targeted sites also provide potential mechanisms to perturb the stability and function of JPH2 protein (Fig. 1C, 2C and 2F).

AAV-mediated mosaic infection avoids cardiomyopathies caused by JPH2 depletion

To determine the effect of AAV dosage on whole organ and individual CM phenotypes, we treated mice with serial dilutions of AAV-gRNA(Jph2)1+2-TNT-Cre, referred to subsequently as AAV-gRNA(Jph2), at P1. We defined the mice receiving 1.1×10^{9}vg/g, 6.1×10^{9}vg/g, 1.8×10^{10}vg/g, and 5.5×10^{10}vg/g AAV doses as Jph2_Low, Jph2_Mid, Jph2_High, and Jph2_Full groups, respectively. We measured the frequency of transduced CMs at P7 by detecting Cre-dependent GFP expression from the *Rosa26*$^{Cas9\text{-}GFP}$ allele. AAV dose was positively correlated to the myocardial area occupied by GFP^{+} CMs (Fig. 3A). We quantified the frequency of GFP^{+} CMs in dissociated CM preparations. Jph2_Low, Jph2_Mid, Jph2_High, and Jph2_Full groups expressed GFP in 22%, 47%, 64%, and 75% of CMs, respectively (Fig. 3B).

Next we investigated whether AAV dosage influences the efficiency of JPH2 depletion in individual transduced CMs. We performed immunofluorescence staining of JPH2 in CMs that were treated with different AAV doses at P1 and isolated at P7. The control AAV-TNT-Cre virus (lacking gRNA) was administered at the full dose (5.5×10^{10}vg/g). Immunostaining of JPH2 was used to measure each cell's JPH2 expression level, and immunostaining of caveolin-3 (CAV3), a plasma membrane marker, defined the boundary of each single cell (Fig. 3C–D). We found a ~70% decrease of JPH2 intensity in Jph2-CASAAV-treated CMs as compared to negative controls, which further confirmed the efficient depletion of JPH2 protein. By immunostaining, there was no detectable difference in intensity between GFP^{+} CMs that were treated with different doses of AAVs (Fig. 3D). To examine the effect of AAV dose on gene depletion efficiency, we FACS-sorted GFP^{+} cells in each group and analyzed JPH2 expression by Western blotting (Fig. 3E). This demonstrated efficient JPH2 depletion in all groups, although the protein remained detectable in the Jph2_Low and Jph2_Mid groups but was undetectable in the Jph2_High and Jph2_Full groups. Thus, AAV dose primarily determines the frequency of transduced CMs. The dose has a small effect on protein depletion efficiency among transduced cells, but even at the lowest dose tested the protein was efficiently depleted. These findings are important for interpreting the mosaic gene knockout data presented below.

Mice that received the full dose of AAV-gRNA(Jph2) died between P10–P13 (Fig. 4A), which is consistent with the survival curve of Myh6-Cre;Jph2-shRNA mice described previously[8]. Mice treated with the other doses of AAV-gRNA(Jph2) survived beyond P20 (Fig. 4A), when T-tubules become fully mature[2]. Because our goal was to examine the impact of Jph2 on T-tubule maturation, we focused the following studies on Jph2_Low, Jph2_Mid and Jph2_High groups and studied mice at P21–P24. Analyses of gross heart morphology showed that Jph2_High and Jph2_Mid groups had cardiac hypertrophy and dilatation, which were not evident in the Jph2_Low group (Fig. 4B). This difference was

quantified by measurement of the heart weight to body weight ratio (HW/BW), which was not elevated in the Jph2_Low group but was increased in Jph2_Mid and Jph2_High groups in a dose-dependent manner (Fig. 4C). Echocardiography showed severely depressed heart systolic function in the Jph2_High group (Fig. 4D). By contrast, the Jph2_Mid group had moderately depressed heart function, and the Jph2_Low group did not exhibit detectable heart dysfunction (Fig. 4D). AAV-gRNA(Jph2) dosage also correlated with the extent of left ventricular dilatation (Fig. 4E–F). Expression of cardiac stress markers *Myh7*, *Nppa*, and *Nppb* were consistent with these overall effects of virus dose on heart structure and functions (Fig. 4G). Together, these data indicate that high and mid doses of AAV-gRNA(Jph2) caused dose-related cardiac hypertrophy and dysfunction, as previously reported in *Jph2* shRNA genetic mouse models[2,8], while the low dose did not impact heart function at the organ level.

We next examined the effect of the extent of *Jph2* inactivation on the responses of individual CMs. While induction of heart dysfunction correlated with increased CM size, there was no difference in CM size between GFP^+ and GFP^- CMs at any viral dose (Fig. 4H). Thus JPH2 depletion does not directly affect CM size. Rather, JPH2 affects CM size indirectly through effects on overall organ function.

Collectively, these data show that a low dose of AAV-gRNA(Jph2) can be used to achieve mosaic depletion of JPH2 without affecting overall organ function. Mid and high doses increase the fraction of cardiac myocytes with gene inactivation and correspondingly cause organ dysfunction and global stress responses.

JPH2 plays a minor role in T-tubule maturation

Because mosaic *Jph2* inactivation by low-dose AAV-gRNA(Jph2) avoided secondary effects of organ dysfunction, we were able to precisely examine the role of JPH2 in T-tubule organization without the confounding effects of cardiac dysfunction. To observe T-tubule organization in live CMs in intact heart ventricles, we labeled T-tubules with the plasma membrane dye FM 4-64 through retrograde heart perfusion and performed *in situ* confocal imaging[2,30]. We found that T-tubules were dramatically disrupted in GFP^+ CMs in Jph2_High mice. However, this phenotype was mild in GFP^+ CMs in Jph2_Mid mice. No overt disruption in T-tubules was observed in GFP^+ CMs in Jph2_Low mice (Fig. 5A–B; see additional representative confocal z-stacks in Online Movies I–III). We analyzed the changes in T-tubules in details by performing unbiased quantification of T-tubule morphology using AutoTT software[20] (Fig. 5B). This software objectively quantifies transverse T-tubule elements (TEs), longitudinal T-tubule elements (LEs), total T-tubule elements (which equal to TEs+LEs), and T-tubule regularity[20]. Compared to GFP^- internal control CMs, GFP^+ CMs in Jph2_Low group showed no significant change in T-tubule regularity or LEs, and subtly but significantly reduced TEs and total T-tubule elements (Fig. 5C–F). The Jph2_Mid group also showed no significant change in LEs, but a significant impairment in the other three parameters that was greater than in the Jph2_Low group. All of these parameters were most dramatically impaired in the Jph2_High group. T-tubules in GFP^- CMs from Jph2_High mice exhibited T-tubule defects, which were more severe than GFP^+ CMs in Jph2_Low and Jph2_Mid mice. These data are consistent with prior observations that T-

tubules remodel and become disorganized in wild-type CMs in pathological conditions[9]. The GFP$^+$ CMs in Jph2_High mice had substantially more disrupted T-tubules than their GFP$^-$ counterparts (Fig. 5C–F), suggesting a cell-autonomous role for JPH2 to protect T-tubules from remodeling in heart failure[31]. We also examined the effect of JPH2 depletion on sarcomere structure, as assessed by immunostaining for Z-line marker sarcomeric α-actinin (Actn2; Online Fig. V). Z-line spacing and regularity, measured by AutoTT[20], were not significantly affected by JPH2 depletion (Online Fig. V). Together these data demonstrate that JPH2 has a minor cell-autonomous function in T-tubule organization that is exacerbated by heart failure.

To further confirm that these varied phenotypes were not caused by JPH2 depletion efficiency, we performed dual-color immunofluorescence to detect both JPH2 and CAV3 in CMs dissociated from AAV-TNT-Cre (control) and AAV-gRNA(Jph2)-treated mice. This permitted us to identify true JPH2-deficient CMs and examine CAV3 pattern in these CMs (Fig. 6A). Consistent with *in situ* T-tubule imaging results, JPH2$^-$ CMs that were derived from Jph2_Low mice exhibited normal global T-tubule morphology as compared to JPH2$^+$ control CMs (Fig. 6A). By contrast, Jph2_Mid and Jph2_High mice exhibited disrupted CAV3 patterns in JPH2$^-$ CMs (Fig. 6A). AutoTT quantification of CAV3 immunostaining also showed significantly decreased total T-tubule elements as well as regularity in JPH2$^-$ CMs isolated from Jph2_Mid and Jph2_High mice, but no statistically significant difference between Jph2_Low and control was observed (Fig. 6B–C). It is possible that this experiment did not reproduce the mild T-tubule defects in Jph2_Low that were observed by *in situ* T-tubule imaging (Fig. 5) because the CM dissociation procedure affects T-tubule organization in some CMs and thereby increases within-group variation (compare error bars between Fig. 5 and Fig. 6). However, based on both *in situ* T-tubule analysis and CAV3 analysis on isolated CMs, it is clear that JPH2 has a minor direct function in T-tubule maturation. Substantial T-tubule disruption was only observed when JPH2 was depleted in a large fraction of CMs, resulting in cardiac stress and associated secondary effects on CMs (Fig. 6D).

We next evaluated whether the varied effect of JPH2 depletion on T-tubule organization influences Ca^{2+} handling. Freshly dissociated CMs were loaded with the Ca^{2+}-sensitive dye Rhod-2 AM, and Ca^{2+} transients were measured by confocal line scan imaging. Both transduced and non-transduced Jph2_High CMs exhibited significantly reduced Ca^{2+} transient amplitude, prolonged time to peak, and slower time to 50% decay (Fig. 7A–B), which is consistent with prior studies of JPH2's role in Ca^{2+} handling[32]. However, the major effect was likely secondary to heart failure and not directly attributable to JPH2 depletion, since the difference with TNT-Cre control and Jph2_High CMs was greater than the difference between GFP+ and GFP- CMs within Jph2_High. Ca^{2+} transient amplitude was more severely depressed in GFP$^+$ than GFP$^-$ Jph2_High CMs, consistent with the more severe T-tubule abnormalities observed in GFP$^+$ vs GFP$^-$ Jph2_High CMs. Jph2_Low GFP$^+$ CMs had Ca^{2+} transients with mildly but significantly reduced peak amplitude compared to GFP$^-$ CMs isolated from the same heart. No significant change in time to peak or time to 50% decay was detected (Fig. 7C–D). This is consistent with the minor effect of JPH2 depletion on T-tubule morphology in Jph2_Low. These single-cell measurements of Ca^{2+}

handling paralleled our imaging data on T-tubule structure, and indicate that JPH2 has a minor cell-autonomous role in establishing Ca^{2+} release unit function.

CASAAV-based screen identifies RYR2 as a novel T-tubule regulator

Mosaic mutagenesis by CASAAV avoids the time-consuming procedure of generating genetically modified mice. A large number of AAVs that deliver gRNAs directed at different genes can be generated side-by-side simultaneously. Thus, this technology allowed us to perform a genetic screen for novel T-tubule regulators. Using a candidate-based approach, we generated AAVs targeting 8 genes that could be potentially important for T-tubule maturation. These genes encode important cardiac transcriptional factors (NKX2-5, TBX5, MEF2C and TEAD1) as well as T-tubule-associated proteins (RYR2, CACNA1C, CAV3 and NCX1). We injected each of these viruses into P1 $Rosa26^{Cas9\text{-}P2A\text{-}GFP}$ mice at a low dose (similar to that used in Jph2_Low), dissociated the hearts at P21, and performed JPH2 immunostaining to image T-tubule morphology in GFP^+ CMs (Fig. 8A). GFP^- CMs from the same heart were used as internal negative controls. Efficient depletion of NKX2-5, TEAD1, RYR2 and CAV3 were validated by immunostaining (Online Fig. VI; see also Fig. 8C–D).

Through this screen, we found that RYR2 depletion caused dramatic disruption of the JPH2 staining pattern (Fig. 8A–B). By contrast, the AAVs targeting the other 7 genes did not show this effect. Efficient depletion of RYR2 was observed in ~65% of the AAV-infected GFP^+ CMs (Fig. 8C–D). Mice with mosaic RYR2 depletion in a minority of CMs (only ~10% of total CMs were depleted of RYR2) maintained normal heart function (Fig. 8E). Dramatic T-tubule disruption was observed in GFP^+ CMs under *in situ* T-tubule imaging, but GFP^- neighboring cells retained normal T-tubule patterns (Fig. 8F–G; see additional representative confocal z-stacks in Online Movie IV). This phenotype was also confirmed in isolated CMs, as $RYR2^-$ CMs exhibited disrupted CAV3 staining pattern while normal CAV3 pattern was observed in $RYR2^+$ CMs (Fig. 8H–I). The effect of RYR2 depletion on T-tubule structure staining pattern was reproduced with two additional independent pairs of gRNAs (Online Fig. VII), which ruled out off-target effects. Together, these data show a novel cell-autonomous function of RYR2 in T-tubule maturation.

DISCUSSION

In this study, we combined AAV-mediated mosaic transduction and CRISPR/Cas9-based somatic mutagenesis to establish a powerful technical platform, named CASAAV, which permits facile interrogation of cell-autonomous gene function in the postnatal heart. We also demonstrate the value of a genetic mosaic strategy to disentangle direct, cell-autonomous roles of a gene from changes that arise from effects on overall organ function. We anticipate that this strategy will allow the rapid and precise interrogation of gene function in the postnatal heart in diverse processes such as CM maturation, regeneration, and hypertrophy.

Somatic cardiac mutagenesis using a Cre-activated *Myh6-Cas9* allele was described previously[24]. Our study used the more widely available $Rosa26^{Cas9\text{-}GFP}$ mouse line[14], which retains cardiac myocyte-selective gene inactivation in the heart due to the cardiotrophic properties of AAV9 and cTNT-Cre-driven Cas9 activation. More importantly, our study

focused on mosaic analysis of cell-autonomous phenotypes as a strength of the Cas9 somatic mutagenesis strategy. We performed foundational experiments that are required to fully exploit this strategy, including the demonstration that the dose of AAV mainly affects the frequency of transduced CMs but has only a small effect on the efficiency of gene inactivation among those CMs that are transduced. Furthermore, we provide data on the overall knockout efficiency of the system, demonstrate that tandem gRNAs targeting the same gene enhances knockout efficiency, and reveal the combination of mechanisms that collectively ensure a high knockout efficiency.

We combined CASAAV with *in situ* T-tubule imaging to study the genetic regulation of CM maturation in vivo. At a full virus dose to maximize the transduction of CMs, CASAAV fully recapitulated observations made using more traditional genetic models. For example, when JPH2 was depleted in a large fraction of CMs (Jph2_High and Jph2_Full), the heart exhibited ventricular dilatation, CM hypertrophy, and heart failure, which were all consistent with previous studies of *Mhy6-Cre; Jph2-shRNA* mice[2,8]. Dramatic T-tubule defects and Ca^{2+} transient abnormalities in Jph2_High mice also agreed with previous reports showing that organ-wide JPH2 knockdown caused heart failure and disrupted T-tubule organization and Ca^{2+} handling[2,8]. Thus this technology can faithfully detect the function of a given gene at both organ and single-cell levels, which provides an alternative and more rapid means to study the function of a given gene in the heart, compared to generation of transgenic or knockout mice.

A particular strength of the CASAAV system is the ability to rapidly generate genetic mosaics, which permits precise delineation of gene function that is difficult to achieve using constitutive or even inducible knockout models. For example, because JPH2 depletion caused early-onset heart failure, which itself is associated with T-tubule disruption, studies in traditional JPH2 knockout mice were unable to disentangle the direct role of JPH2 on T-tubule maturation from its role to stabilize T-tubules in the face of cardiac dysfunction. By using a low dose of AAV to direct JPH2 depletion, we were able to separate the function of JPH2 in T-tubule maturation from its requirement to stabilize T-tubules in heart failure. In CMs from Jph2_Low mice that lacked JPH2 but had overall preserved heart function, we observed very mild T-tubule defects. However, as we increased the fraction of CMs that lack JPH2, we observed worsening T-tubule defects in both transduced and non-transduced CMs that paralleled the extent of heart dysfunction. These observations are consistent with previous studies[31,32] and suggest that widespread JPH2 depletion primarily affects T-tubule organization by impairing heart function. In failing hearts, we did observe that JPH2-depleted CMs had more severe T-tubule disruption than JPH2-replete CMs, supporting a role for JPH2 to stabilize T-tubules in the face of CM stress caused by heart dysfunction, as previously reported[31]. However, contrary to prior studies of JPH2 depletion done in the context of heart dysfunction[2,8], our genetic mosaic approach shows that JPH2 has a minor cell-autonomous role in T-tubule maturation. This role of JPH2 was mirrored in its modest but measurable effects on Ca^{2+} transient amplitude, which suggests that JPH2 may regulate RYR2 activation within Ca^{2+} release units. A broader implication of these results is that studies of CM maturation or function need to use strategies such as genetic mosaicism to distinguish direct cell-autonomous gene function from effects of gene inactivation that occur secondary to organ function impairment.

Another advantage of performing mosaic mutagenesis is that it permits study of genes that are essential for animal survival. For example, because RYR2 is the core Ca^{2+} channel that directly drives heart contraction, RYR2 knockout rapidly causes embryonic death[33], precluding its detailed functional analysis in vivo in the postnatal heart. By contrast, through AAV-based mosaic knockout, we were able to study the in vivo function of RYR2 in adult CMs while maintaining normal heart function. This provided us with the unprecedented opportunity to identify a novel role of RYR2 in T-tubule organization. Thus the CASAAV platform opens the door to precisely investigate the cellular functions of essential genes in vivo, which otherwise would be technically inaccessible.

Our in vivo screen identified RYR2 as a previously undescribed regulator of T-tubule maturation. Further experiments will be required to define how RYR2 regulates T-tubule maturation. One possibility is that RYR2, located on junctional SR, serves a structural role by providing a scaffold that interacts with proteins on T-tubules. Another possibility is that normal Ca^{2+} oscillations conducted through RYR2 are required to promote formation and maturation of T-tubules.

Because CRISPR/Cas9 provides the versatility to target most genes in the genome and CASAAV avoids the time and resources required to generate genetically modified mice, this technology greatly expedites the use of genetic loss-of-function strategies to study gene function in the postnatal heart. In our hands, the whole procedure from gene selection to phenotypic characterization of T-tubules in knockout CM can be done within 6 weeks. As a result, we were able to perform the in vivo screen that led to identification of RYR2 as a novel T-tubule regulator. Thus this technology is well suited for in vivo genetic screening for regulators of CM phenotypes, such as maturation and hypertrophy.

Adenoviral and AAV-mediated delivery of short hairpin RNAs (shRNAs) have been previously used to knockdown genes in postnatal cardiac myocytes. Compared to short hairpin RNAs, CASAAV has clear advantages. ShRNAs are unable to achieve complete protein depletion, and greater than 70% depletion is often considered successful knockdown. ShRNAs must actively bind to target transcripts, so that knockdown depends on continued shRNA expression at sufficient levels compared to the endogenous transcript. With CASAAV, a subset of cells with homozygous truncating mutations will have complete protein depletion. Furthermore, CASAAV irreversibly modifies the genome, which makes gene knockdown irreversible, more potent than shRNAs, and likely accounts for the relative insensitivity of gene depletion efficiency among transduced cells to overall viral dose, a critical feature for the mosaic strategy.

The CASAAV system has some limitations. First, we are unaware of efficient homology-directed repair in terminally differentiated cells, making targeted knock-in mutations infeasible. Second, as with siRNA knockdown strategies, one should be cognizant of potential off-target activity and control for this possibility by careful gRNA design and, optimally, use of two or more independent gRNA pairs to target the same gene. Third, the possibility of gain-of-function mutations should be considered, e.g. if the gRNA leads to C-terminal truncation and a dominant negative N-terminal protein fragment. We used gRNAs targeting near the N-terminus of genes to minimize this possibility. Fourth, for the mosaic

strategy to be successful, one needs means to identify individual cells that have undergone gene inactivation. Immunostaining with a high quality antibody is one such assay. Alternatively, if the fraction of cells that have undergone gene depletion is sufficiently high, one can use GFP from *Rosa26*$^{Cas9\text{-}GFP}$ as a surrogate marker. When doing so, one should also be aware that a low fraction of GFP negative cells also could have undergone Cas9 mutagenesis but have lost GFP expression. Typically this can be overcome by studying a large number of single cells.

In summary, we have developed a rapid and powerful technical platform for gene inactivation in postnatal CMs. This platform is particularly well suited for genetic mosaic analysis of genes to define the cell-autonomous functions. In the future, we anticipate that the capabilities of this system will be further extended by pairing it with single-cell functional phenotyping and single-cell RNA-seq.

Supplementary Material

Refer to Web version on PubMed Central for supplementary material.

Acknowledgments

SOURCES OF FUNDING

The project was supported by UM1 HL098166, R01 HL116461, and U01HL131003 from the National Heart, Lung, and Blood Institute. LSS was supported by R01HL090905 and R01HL130464. NJV was supported by T32HL007572 and F32HL13423501. SG was a recipient of a Coordenação de Aperfeiçoamento de Pessoal de Nível Superior fellowship and funded by Conselho Nacional de Desenvolvimento Científico e Tecnológico and Fundação de Amparo a Pesquisa do Estado de Minas Gerais. The content is solely the responsibility of the authors and does not necessarily represent the official views of the National Heart, Lung, and Blood Institute or the National Institutes of Health.

Nonstandard Abbreviations and Acronyms

CM	Cardiac myocyte
AAV	Adeno-associated virus
CRISPR	Clustered regularly interspaced short palindromic repeats
CASAAV	CRISPR/Cas9-AAV9-based somatic mutagenesis
T-tubule	Transverse Tubule
JPH2	Junctophilin-2
RYR2	Ryanodine Receptor-2

References

1. Yang X, Pabon L, Murry CE. Engineering adolescence: maturation of human pluripotent stem cell-derived cardiac myocytes. Circ Res. 2014; 114:511–523. [PubMed: 24481842]
2. Chen B, Guo A, Zhang C, Chen R, Zhu Y, Hong J, Kutschke W, et al. Critical roles of junctophilin-2 in T-tubule and excitation–contraction coupling maturation during postnatal development. Cardiovasc Res. 2013; 100:54–62. [PubMed: 23860812]

3. Sallé L, Brette F. T-tubules: a key structure of cardiac function and dysfunction. Arch Mal Coeur Vaiss. 2007; 100:225–230. [PubMed: 17536428]

4. Orchard C, Brette F. t-Tubules and sarcoplasmic reticulum function in cardiac ventricular myocytes. Cardiovasc Res. 2008; 77:237–244. [PubMed: 18006490]

5. Beavers DL, Landstrom AP, Chiang DY, Wehrens XHT. Emerging roles of junctophilin-2 in the heart and implications for cardiac diseases. Cardiovasc Res. 2014; 103:198–205. [PubMed: 24935431]

6. Landstrom AP, Beavers DL, Wehrens XHT. The junctophilin family of proteins: from bench to bedside. Trends Mol Med. 2014; 20:353–362. [PubMed: 24636942]

7. Takeshima H, Komazaki S, Nishi M, Iino M, Kangawa K. Junctophilins: a novel family of junctional membrane complex proteins. Mol Cell. 2000; 6:11–22. [PubMed: 10949023]

8. Reynolds JO, Chiang DY, Wang W, Beavers DL, Dixit SS, Skapura DG, Landstrom AP, et al. Junctophilin-2 is necessary for T-tubule maturation during mouse heart development. Cardiovasc Res. 2013; 100:44–53. [PubMed: 23715556]

9. Wei S, Guo A, Chen B, Kutschke W, Xie Y-P, Zimmerman K, Weiss RM, et al. T-tubule remodeling during transition from hypertrophy to heart failure. Circ Res. 2010; 107:520–531. [PubMed: 20576937]

10. Poláková E, Sobie EA. Alterations in T-tubule and dyad structure in heart disease: challenges and opportunities for computational analyses. Cardiovasc Res. 2013; 98:233–239. [PubMed: 23396602]

11. Prendiville TW, Guo H, Lin Z, Zhou P, Stevens SM, He A, VanDusen N, et al. Novel Roles of GATA4/6 in the Postnatal Heart Identified through Temporally Controlled, Cardiac myocyte-Specific Gene Inactivation by Adeno-Associated Virus Delivery of Cre Recombinase. PLoS One. 2015; 10:e0128105. [PubMed: 26023924]

12. Swiech L, Heidenreich M, Banerjee A, Habib N, Li Y, Trombetta J, Sur M, et al. In vivo interrogation of gene function in the mammalian brain using CRISPR-Cas9. Nat Biotechnol. 2015; 33:102–106. [PubMed: 25326897]

13. Lin Z, von Gise A, Zhou P, Gu F, Ma Q, Jiang J, Yau AL, et al. Cardiac-specific YAP activation improves cardiac function and survival in an experimental murine MI model. Circ Res. 2014; 115:354–363. [PubMed: 24833660]

14. Platt RJ, Chen S, Zhou Y, Yim MJ, Swiech L, Kempton HR, Dahlman JE, et al. CRISPR-Cas9 knockin mice for genome editing and cancer modeling. Cell. 2014; 159:440–455. [PubMed: 25263330]

15. O'Connell, TD., Rodrigo, MC., Simpson, PC. Isolation and Culture of Adult Mouse Cardiac Myocytes. In: Vivanco, F., editor. Cardiovascular Proteomics. Humana Press; p. 271-296.

16. He A, Pu WT. Genome-wide location analysis by pull down of in vivo biotinylated transcription factors. Curr Protoc Mol Biol. 2010; Chapter 21(Unit 21.20)

17. Pinello L, Canver MC, Hoban MD, Orkin SH, Kohn DB, Bauer DE, Yuan G-C. Analyzing CRISPR genome-editing experiments with CRISPResso. Nat Biotechnol. 2016; 34:695–697. [PubMed: 27404874]

18. Guo Y, Zheng Y. Lamins position the nuclear pores and centrosomes by modulating dynein. Mol Biol Cell. 2015; 26:3379–3389. [PubMed: 26246603]

19. Guo Y, Kim Y, Shimi T, Goldman RD, Zheng Y. Concentration-dependent lamin assembly and its roles in the localization of other nuclear proteins. Mol Biol Cell. 2014; 25:1287–1297. [PubMed: 24523288]

20. Guo A, Song L-S. AutoTT: automated detection and analysis of T-tubule architecture in cardiac myocytes. Biophys J. 2014; 106:2729–2736. [PubMed: 24940790]

21. Jinek M, Chylinski K, Fonfara I, Hauer M, Doudna JA, Charpentier E. A Programmable Dual-RNA–Guided DNA Endonuclease in Adaptive Bacterial Immunity. Science. 2012; 337:816–821. [PubMed: 22745249]

22. Cong L, Ran FA, Cox D, Lin S, Barretto R, Habib N, Hsu PD, et al. Multiplex genome engineering using CRISPR/Cas systems. Science. 2013; 339:819–823. [PubMed: 23287718]

23. Mali P, Yang L, Esvelt KM, Aach J, Guell M, DiCarlo JE, Norville JE, et al. RNA-guided human genome engineering via Cas9. Science. 2013; 339:823–826. [PubMed: 23287722]

24. Carroll KJ, Makarewich CA, McAnally J, Anderson DM, Zentilin L, Liu N, Giacca M, et al. A mouse model for adult cardiac-specific gene deletion with CRISPR/Cas9. Proc Natl Acad Sci U S A. 2016; 113:338–343. [PubMed: 26719419]

25. Pacak CA, Mah CS, Thattaliyath BD, Conlon TJ, Lewis MA, Cloutier DE, Zolotukhin I, et al. Recombinant adeno-associated virus serotype 9 leads to preferential cardiac transduction in vivo. Circ Res. 2006; 99:e3–9. [PubMed: 16873720]

26. Sander JD, Joung JK. CRISPR-Cas systems for editing, regulating and targeting genomes. Nat Biotechnol. 2014; 32:347–355. [PubMed: 24584096]

27. Hong T, Yang H, Zhang S-S, Cho HC, Kalashnikova M, Sun B, Zhang H, et al. Cardiac BIN1 folds T-tubule membrane, controlling ion flux and limiting arrhythmia. Nat Med. 2014; 20:624–632. [PubMed: 24836577]

28. Mamanova L, Coffey AJ, Scott CE, Kozarewa I, Turner EH, Kumar A, Howard E, et al. Target-enrichment strategies for next-generation sequencing. Nat Methods. 2010; 7:111–118. [PubMed: 20111037]

29. Chang Y-F, Imam JS, Wilkinson MF. The nonsense-mediated decay RNA surveillance pathway. Annu Rev Biochem. 2007; 76:51–74. [PubMed: 17352659]

30. Chen B, Zhang C, Guo A, Song L-S. In situ single photon confocal imaging of cardiac myocyte T-tubule system from Langendorff-perfused hearts. Front Physiol. 2015; 6:134. [PubMed: 25999861]

31. Guo A, Zhang X, Iyer VR, Chen B, Zhang C, Kutschke WJ, Weiss RM, et al. Overexpression of junctophilin-2 does not enhance baseline function but attenuates heart failure development after cardiac stress. Proc Natl Acad Sci U S A. 2014; 111:12240–12245. [PubMed: 25092313]

32. Chen B, Guo A, Zhang C, Chen R, Zhu Y, Hong J, Kutschke W, et al. Critical roles of junctophilin-2 in T-tubule and excitation-contraction coupling maturation during postnatal development. Cardiovasc Res. 2013; 100:54–62. [PubMed: 23860812]

33. Takeshima H, Komazaki S, Hirose K, Nishi M, Noda T, Iino M. Embryonic lethality and abnormal cardiac myocytes in mice lacking ryanodine receptor type 2. EMBO J. 1998; 17:3309–3316. [PubMed: 9628868]

NOVELTY AND SIGNIFICANCE

What Is Known?

- Genetic knock out or knock down is a critical research strategy, but the commonly used approach requires developing and obtaining a different genetically modified mouse line for each gene, which is a slow process.
- Genetic knock out in the cardiac myocyte compartment often causes cardiac dysfunction, which initiates a panoply of secondary effects that can obscure the direct, cell autonomous effects of gene inactivation.
- Junctaphilin-2 is implicated in development of T-tubules, a hallmark of cardiac myocyte maturation, because knock down of junctophilin-2 using shRNAs causes heart failure and T-tubule disruption.

What New Information Does This Article Contribute?

- We developed a cardiac myocyte selective, Cas9/AAV9-mediated gene inactivation platform, named CASAAV, that allows efficient inactivation of a gene without developing or acquiring a new mouse line for the gene of interest.
- Upon administration of different tilters of AAV constructs, both organ-wide and cell autonomous effects of gene depletion can be studied, allowing dissection of direct cell autonomous effects from the secondary effects due to cardiac dysfunction.
- Applying CASAAV approach to study T-tubule maturation, we found that junctophilin-2 plays a minor cell autonomous role in T-tubule maturation, and we uncovered a novel, cell autonomous role for RYR2 in T-tubule maturation.

Cardiac myocyte-selective genetic loss of function is a powerful strategy for dissecting gene function in the heart. However, implementing this strategy using the traditional approaches is time consuming and results are vulnerable to misinterpretation because of secondary effects caused by organ-wide gene inactivation. Here, we show that a Cas9 and AAV-based platform (CASAAV) permits efficient and rapid gene inactivation, in either a small or large fraction of cardiac myocytes. We deploy this new method to study T-tubule formation, a hallmark of mature cardiac myocytes. Using the CASAAV platform, we show that junctophilin 2, a gene previously found to be essential for T-tubule maturation, has a limited role in this process. A CASAAV candidate-based screen uncovered an unanticipated role for RYR2 in T-tubule formation. The CASAAV platform and the mosaic gene inactivation strategy provide avenues to more rapidly and precisely perform in vivo genetic loss of function studies in cardiac myocytes.

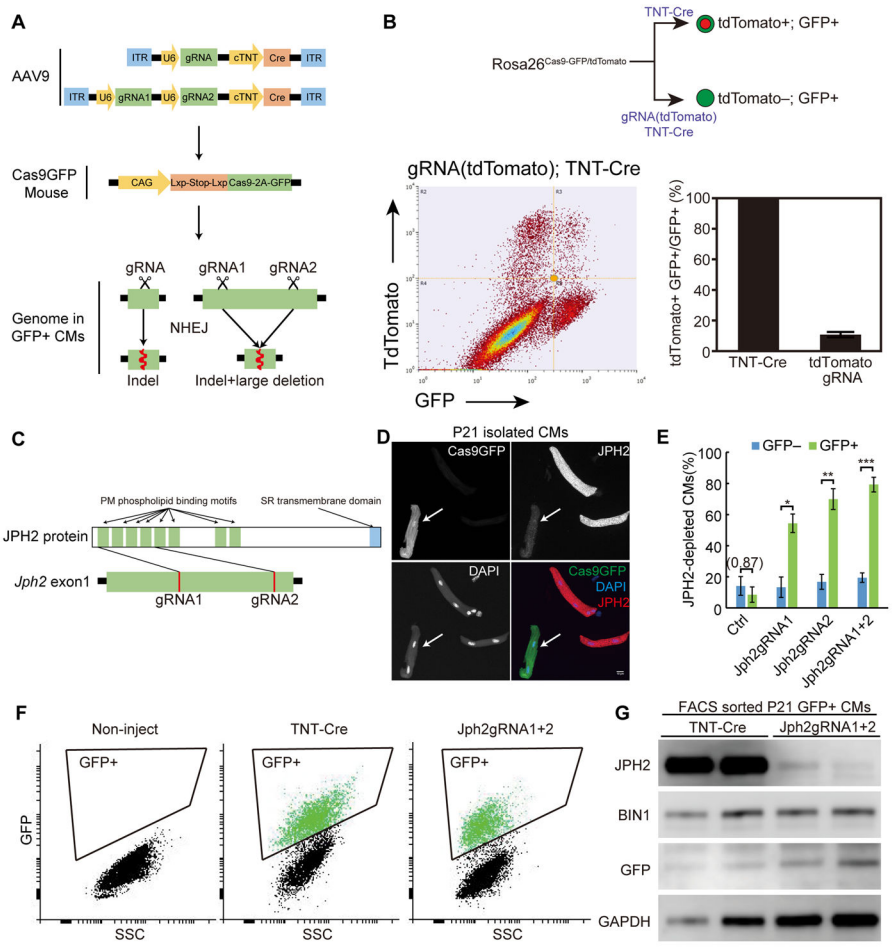

Figure 1. CASAAV-based somatic mutagenesis efficiently depleted Jph2 in CMs during CM maturation in vivo

(A) Workflow for CASAAV. (B) Depletion of tdTomato by AAV9 delivery of specific gRNA plus Cre to activate Cas9-P2A-GFP. Dot plot shows that most GFP$^+$ cells were tdTomato negative. As a control, AAV9 delivery of Cre without gRNA activated tdTomato in almost all GFP$^+$ cells (see also Online Fig. II). (C) Design of Jph2 gRNAs that target the first coding exon of the *Jph2* gene. (D) Immunostaining of JPH2 in isolated CMs demonstrated efficient depletion of JPH2 in Cas9GFP$^+$ CMs (arrow). Scale bar, 10 μm. (E) Quantification of the fraction of JPH2-depleted CMs among GFP$^-$ and GFP$^+$ CMs. >50 CMs were counted per heart. n = 5 hearts. Student's t-test: *p<0.05; **p<0.01; ***p<0.001. Non-significant p value is shown in parentheses. Plots show mean ± SD. (F–G) Depletion of JPH2 in transduced (GFP$^+$) CMs. Gating strategy for FACS purification of isolated GFP$^+$ CMs is shown in F. Panel G shows Western blot analysis of FACS-sorted GFP$^+$ cells.

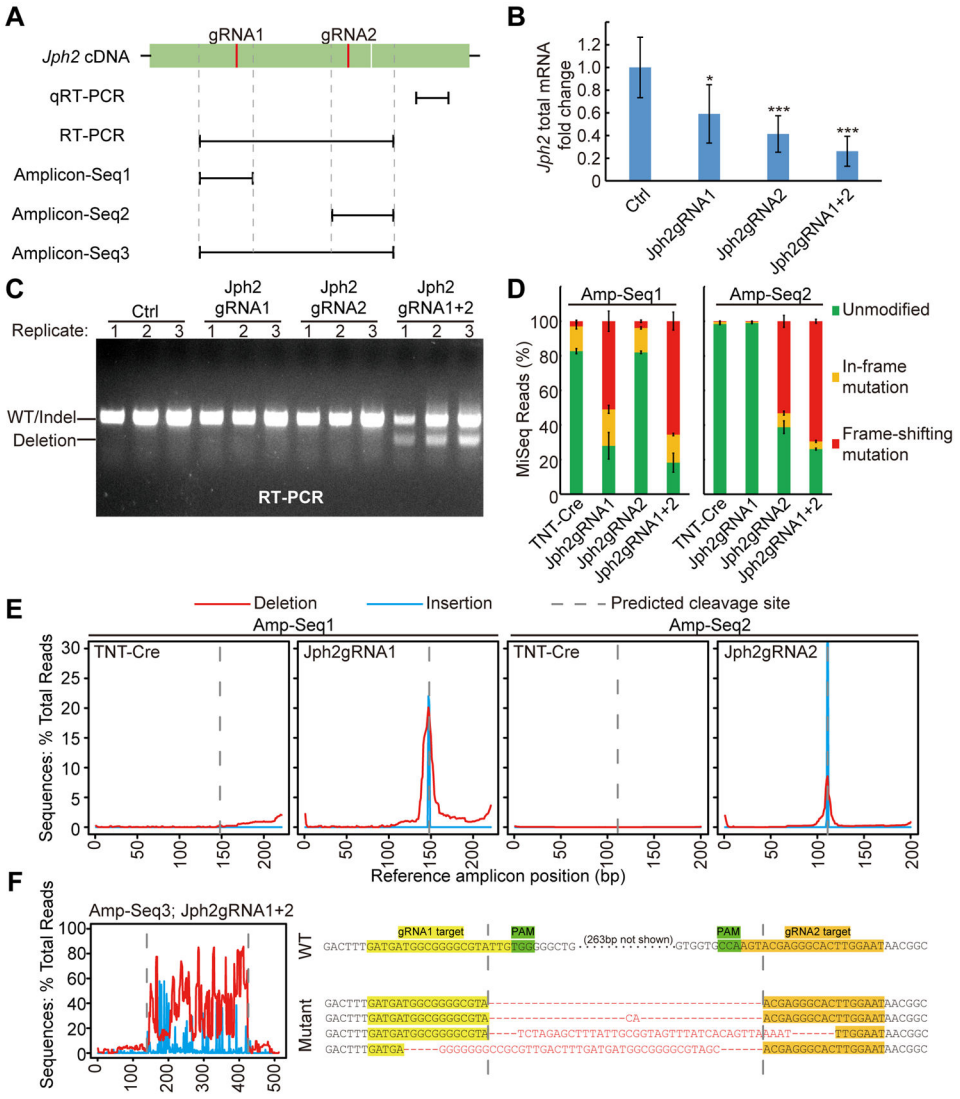

Figure 2. Multiple mechanisms mediate efficient Jph2 depletion in CMs

(A) A scheme of targeted loci on *Jph2* cDNA for qRT-PCR, RT-PCR and Amplicon-Seq analyses. (B) qRT-PCR analysis of *Jph2* mRNA level. n=6 P7 heart apexes. Student's t-test: *p<0.05; **p<0.01; ***p<0.001. (C) Expression of tandem gRNAs induced deletion between the gRNAs. Transcript structure was interrogated by RTPCR. (D) Quantification of in-frame and frame-shifting mutations identified by Amplicon-Seq. n=3 biological replicates. 300~2000 reads were analyzed per sample. (E) Distribution of small insertions and deletions along cDNA amplicon 1 and 2. (F) Analysis of mutation distribution in Amplicon 3 (left) reveals large deletions between gRNA1&2 target sites. Representative sequencing results in amplicon 3 are shown (right). Deleted or unaligned sequences are in red. Plots show mean ± SD in (B) and (D).

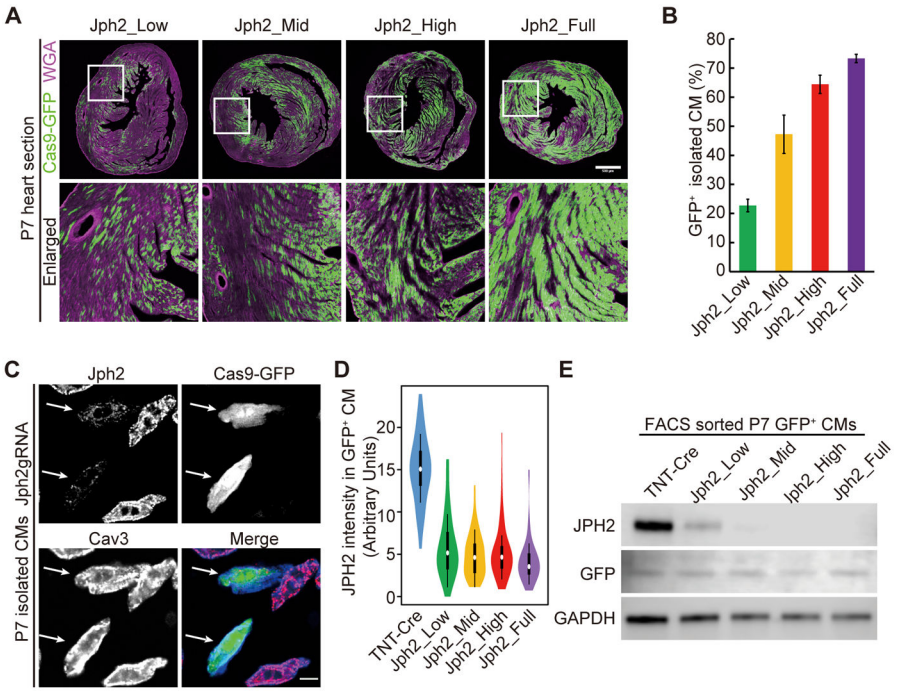

Figure 3. Effect of AAV dosage on the frequency of cardiac myocyte transduction and the extent of JPH2 depletion

(A) Representative images of GFP$^+$ CMs in P7 heart sections that were infected with different doses of AAVs. Scale bar, 500 μm. Boxed area were enlarged at bottom. (B) Quantification of the fraction of GFP$^+$ CMs that were isolated from P7 hearts infected with different doses of AAVs. n = 3 hearts. >400 CMs were counted per heart. (C) Immunostaining of JPH2 in CMs isolated from P7 hearts. Arrows point to GFP$^+$ CMs that were depleted of JPH2. Scale bar, 10 μm. (D) Violin plots of JPH2 immunofluorescence intensity in maximally projected confocal images of P7 CMs. For each group, n = 60 CMs isolated from 3 hearts. White circles and boxes indicate medians and 25th and 75th percentiles. Whiskers extend 1.5 times the interquartile range from the 25th and 75th percentiles. Colored shapes show density estimates of the data. (E). Immunoblot showing level of JPH2 protein GFP+ CMs from the indicated treatment groups.

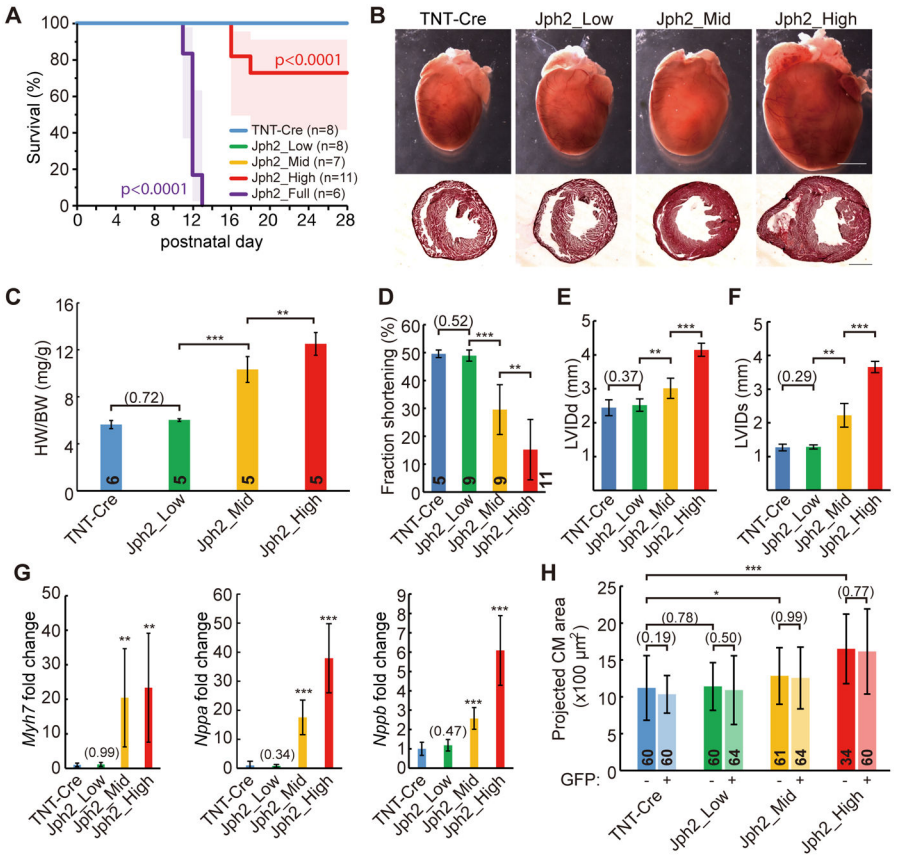

Figure 4. Dose-dependent induction of myocardial dysfunction by AAV-gRNA(Jph2)

(A) Kaplan-Meier analysis of survival curve under control or different doses of Jph2gRNA AAV treatments. (B) Representative whole-heart brightfield images (above) and H&E-stained frozen cross sections (bottom). Scale bar, 2 mm. (C) Heart weight (HW)-body weight (BW) ratio at P21. (D–F) Echocardiographic analysis of heart size and function in P21 mice treated with indicated doses of Jph2gRNA AAV. LVIDd, left ventricular internal diameter end diastole; LVIDs, left ventricular internal diameter end systole. (G) qRT-PCR measurement of heart stress markers. mRNA extracted from P21–P24 heart apexes were analyzed. n=6 hearts. (H) Cell size analysis of isolated CMs. CMs were isolated from 3 hearts in each group. Student's t-test: *p<0.05; **p<0.01; ***p<0.001. Non-significant p values are shown in parentheses. Numbers in bars indicate sample size. Plots show mean ± SD.

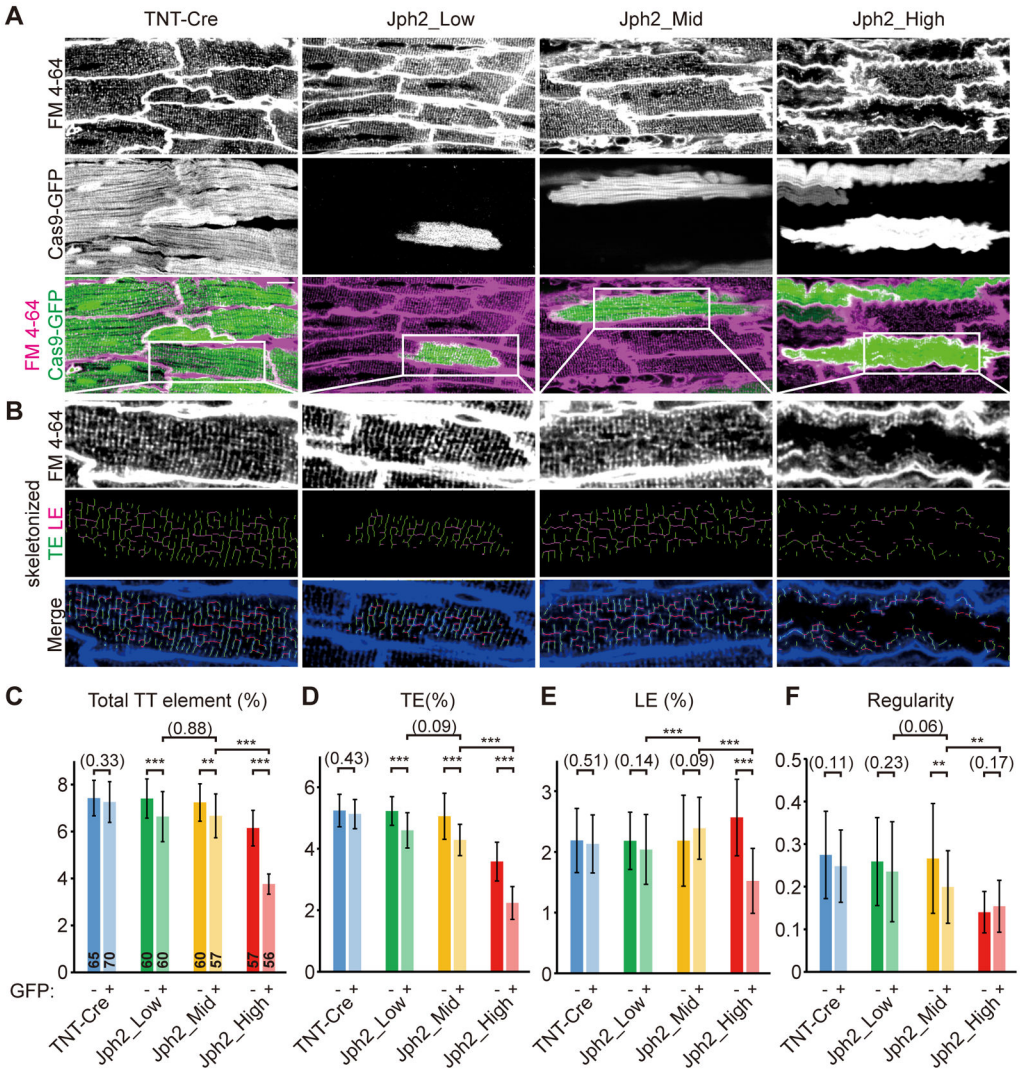

Figure 5. In situ T-tubule analysis of cardiac myocytes with mosaic JPH2 depletion

(A) In situ confocal live imaging of T-tubules in FM4-64-loaded P21 hearts under control or mosaic JPH2 depletion. Scale bar, 20 μm. (B) T-tubule patterns in white boxes in (A) were enlarged and skeletonized. (C–F) AutoTT quantification of T-tubule patterns under in situ imaging. TE, transverse element; LE, longitudinal element; Total TT element=TE+LE. Number of CMs analyzed is shown in columns in panel (C). CMs were dissociated from 3 hearts. Student's t-test: **p<0.01; ***p<0.001. Non-significant p values are shown in parentheses. Plots show mean ± SD.

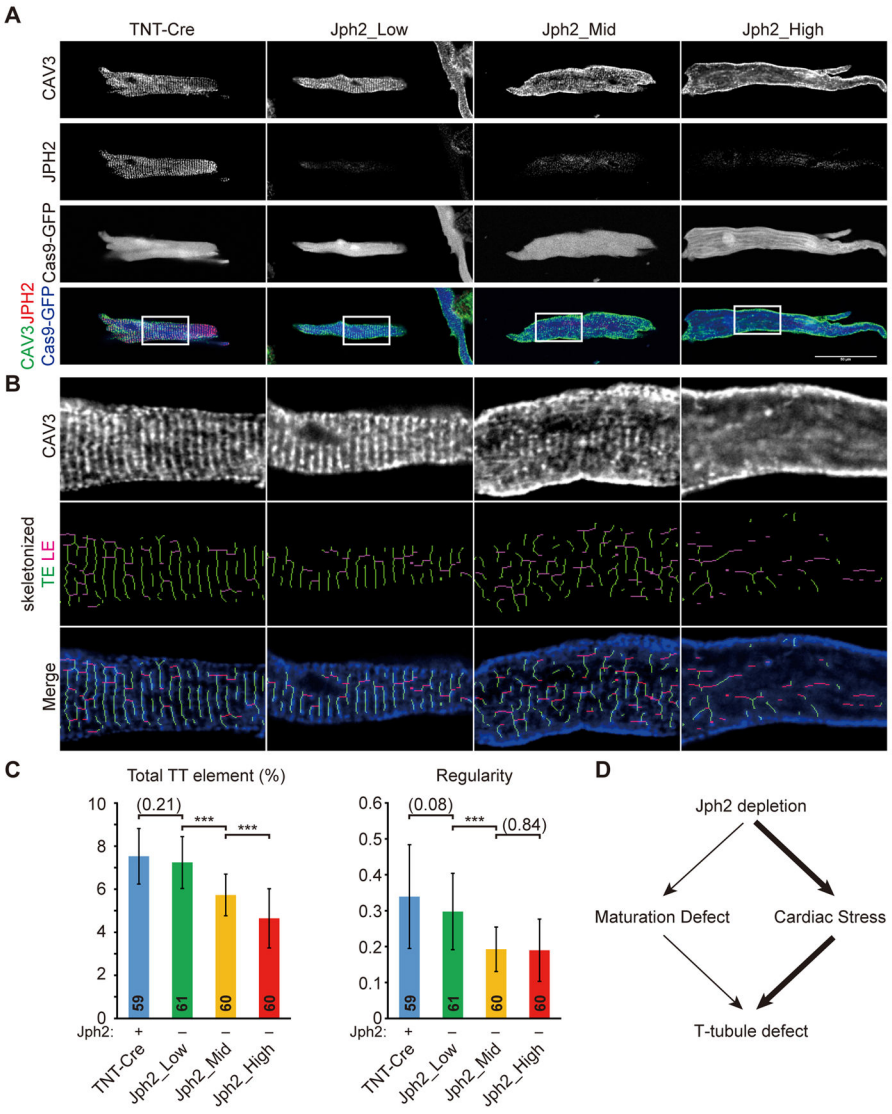

Figure 6. T-tubule analysis in CMs that were isolated from hearts under serial levels of mosaic JPH2 depletion

(A) Representative images of CAV3 and JPH2 staining in CMs isolated from P21 hearts under control or different levels of mosaic JPH2 depletion. Scale bar, 50 μm. CAV3 patterns in white boxes were enlarged and skeletonized in (B). (C) AutoTT quantification of T-tubule patterns in isolated CMs. Number of CMs analyzed was shown in columns in panel (C). CMs were dissociated from 3 hearts per group. Student's t-test: **p<0.01; ***p<0.001. Non-significant p values are shown in parentheses. Plots show mean ± SD. (D). JPH2 depletion had a small cell-autonomous effect of T-tubule structure. Depletion in a large fraction of cardiac myocytes caused heart failure, which indirectly disrupted T-tubule structure.

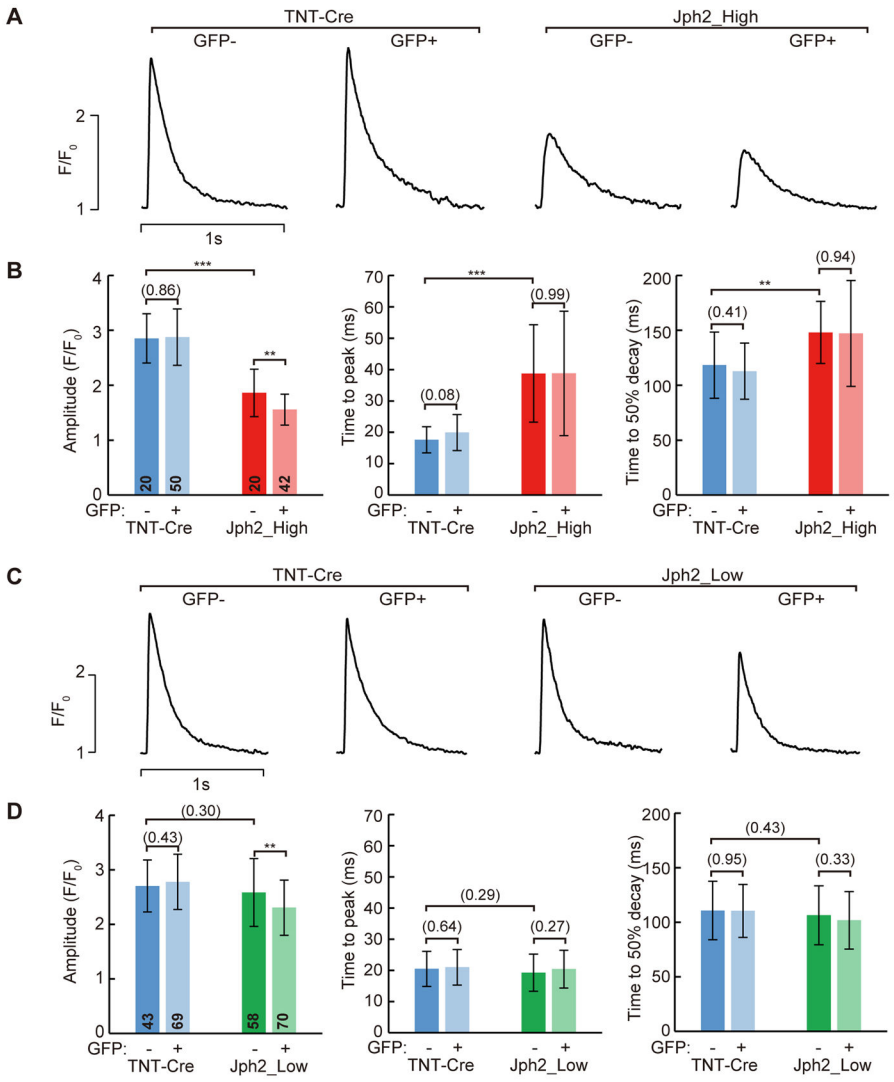

Figure 7. Effect of JPH2 depletion on Ca^{2+} transients in ventricular cardiac myocytes

CMs were dissociated from control, Jph2_High (A–B), or Jph2_Low (C–D) treatment groups. CMs were loaded with the Ca^{2+}-sensitive dye Rhod-2 AM and imaged by confocal line scan. Representative Ca^{2+} transient profiles recorded from cardiac myocytes paced at 1 Hz are shown in A and C, and quantitative data are shown in B and D, plotted as mean ± SD. Number within bars indicates the number of CMs whose data were pooled to calculate the bar. These CMs were isolated from 3 hearts per group. Groups were compared by t-test. **p< 0.01. ***p<0.001. Non-significant p-values are shown in parentheses.

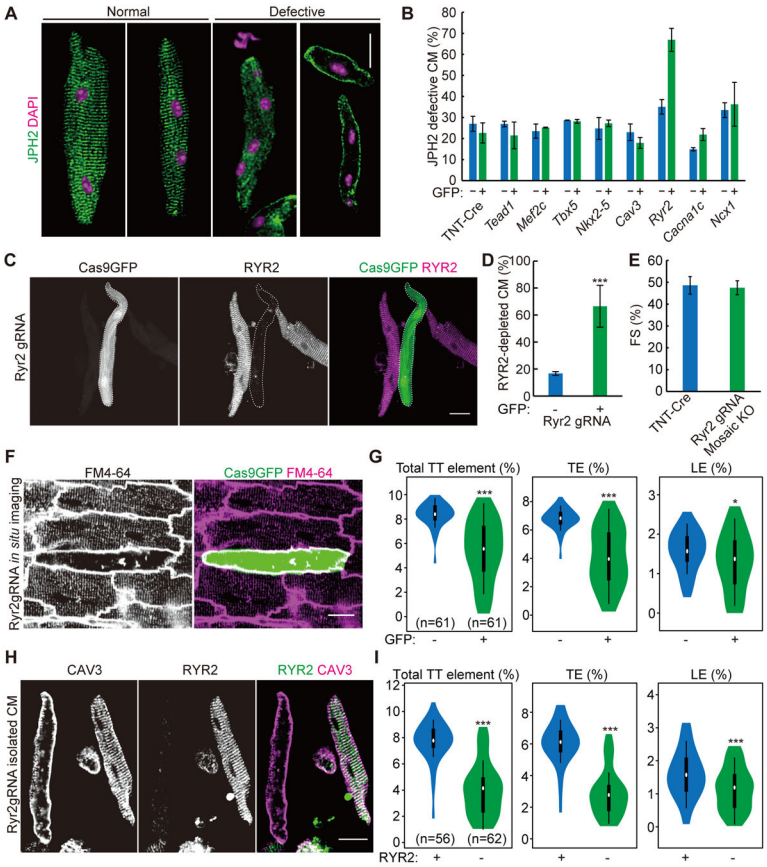

Figure 8. CASAAV-based genetic screen identifies RYR2 as a novel T-tubule regulator

(A) Representative images of JPH2 immunostaining patterns in isolated CMs that demonstrate normal and defective T-tubule organization. (B) Quantification of JPH2 patterns in isolated P21 CMs in which 8 candidate genes were individually and mosaically targeted. >50 CMs were counted per heart. n=3 hearts. (C) Immunostaining of RYR2 demonstrates successful depletion of RYR2 in GFP^{+} CMs (delineated by dashed lines) that are infected by AAV-Ryr2gRNA. (D) Quantification of RYR2 knockout efficiency. >50 CMs were counted per group. n=3 hearts. (E) Fractional shortening (FS) of control and RYR2 mosaic knockout hearts. n=3. (F) in situ T-tubule image of hearts under mosaic RYR2 knockout. (G) AutoTT quantification of RYR2 mosaic knockout CMs. (H) CAV3 and RYR2 immunostaining patterns in CMs isolated from hearts under RYR2 mosaic knockout. (I) AutoTT quantification of CAV3 pattern in RYR2+ and RYR2− isolated CMs. In all images, scale bar=20 μm. Violin plots in panels G and I are as in Fig. 3D. CMs were from 3 hearts. Student's t-test: *p<0.05; **p<0.01; ***p<0.001. Column charts show mean ± SD.